


Transcostal Histotripsy Ablation in an In Vivo Acute Hepatic Porcine Model

Emily A. Knott¹  · Katherine C. Longo¹ · Eli Vlaisavljevich² · Xiaofei Zhang³ · John F. Swietlik¹ · Zhen Xu⁴ · Allison C. Rodgers⁵ · Annie M. Zlevor¹ · Paul F. Laeseke¹ · Timothy L. Hall⁴ · Fred T. Lee Jr¹ · Timothy J. Ziemlewicz¹

Received: 7 January 2021 / Accepted: 28 June 2021 / Published online: 9 July 2021

© Springer Science+Business Media, LLC, part of Springer Nature and the Cardiovascular and Interventional Radiological Society of Europe (CIRSE) 2021

Abstract

Purpose To determine whether histotripsy can create human-scale transcostal ablations in porcine liver without causing severe thermal wall injuries along the beam path.

Materials and Methods Histotripsy was applied to the liver using a preclinical prototype robotic system through a transcostal window in six female swine. A 3.0 cm spherical ablation zone was prescribed. Duration of treatment (75 min) was longer than a prior subcostal treatment study (24 min, 15 s) to minimize beam path heating. Animals then underwent contrast-enhanced MRI, necropsy, and histopathology. Images and tissue were analyzed for ablation zone size, shape, completeness of necrosis, and off-target effects.

Results Ablation zones demonstrated complete necrosis with no viable tissue remaining in 6/6 animals by histopathology. Ablation zone volume was close to prescribed ($13.8 \pm 1.8 \text{ cm}^3$ vs. prescribed 14.1 cm^3). Edema was noted in the body wall overlying the ablation on T2

MRI in 5/5 (one animal did not receive MRI), though there was no gross or histologic evidence of injury to the chest wall at necropsy. At gross inspection, lung discoloration in the right lower lobe was present in 5/6 animals (mean size: $1 \times 2 \times 4 \text{ cm}$) with alveolar hemorrhage, preservation of blood vessels and bronchioles, and minor injuries to pneumocytes noted at histology.

Conclusion Transcostal hepatic histotripsy ablation appears feasible, effective, and no severe injuries were identified in an acute porcine model when prolonged cooling time is added to minimize body wall heating.

Keywords Ultrasound therapy · Ablation techniques · Histotripsy · Interventional oncology · Animal studies

Introduction

Focal tumor ablation is increasingly accepted for the treatment of primary and metastatic liver tumors [1]. However, thermal ablation modalities continue to have limitations including invasiveness, lack of predictability and precision, and the potential to cause thermal injury to vulnerable structures such as bile ducts and bowel [2, 3]. Histotripsy is a non-thermal, non-invasive focused ultrasound ablation modality [4]. High intensity, low duty cycle ultrasound pulses are tightly focused to create acoustic cavitation, destroying targeted tissue at the cellular level [5, 6]. To date, histotripsy has been used in multiple pre-clinical models through a subcostal acoustic window, though never from a fully transcostal approach [7, 8]. It has

✉ Timothy J. Ziemlewicz
tziemlewicz@uwhealth.org

¹ Department of Radiology, University of Wisconsin–Madison, E3/311 CSC, 600 Highland Ave, Madison, WI 53792, USA

² Department of Biomedical Engineering and Mechanics, Virginia Polytechnic Institute and State University, 325 Stanger St, Blacksburg, VA, USA

³ Department of Pathology and Laboratory Medicine, University of Wisconsin–Madison, 600 Highland Ave, Madison, WI, USA

⁴ Department of Biomedical Engineering, University of Michigan, 2200 Bonisteel Blvd, Ann Arbor, MI, USA

⁵ Department of Medicine, University of Wisconsin–Madison, 600 Highland Ave, Madison, WI, USA

produced ablation zones characterized by a high degree of precision, complete destruction of targeted tissue, no body wall damage, and relative preservation of collagen-containing structures with high mechanical strength such as bile ducts, blood vessels, bowel, and urothelium [4–17].

Treatment of high liver lesions and upper pole kidney tumors will require a transcostal acoustic window, which while allowing intermittent intercostal visualization at the target, will lead to partial treatment beam path blockage by the ribcage, potentially resulting in body wall thermal damage [14]. While the treatment site remains non-thermal, the acoustic blockage by the ribs could lead to energy deposition resulting in thermal damage to overlying tissue if not accounted for and properly studied. A prior proof-of-concept study demonstrated limited success in producing a treatment zone of $5 \times 5 \times 5 \text{ mm}^3$, but this is not adequate to treat most tumors and a margin [18]. Whether clinical-scale transcostal ablation zones can be created without causing severe body wall damage is currently unknown. Therefore, the purpose of this study is to investigate transcostal histotripsy using a modified pulse sequence for creating large ablation zones without causing severe body wall damage due to beam path heating.

Materials and Methods

Animal Care, Anesthesia, and Histotripsy

All procedures were approved by the Institutional Animal Care and Use Committee. Six female swine (40–55 kg) were sedated with an intramuscular injection of tiletamine and zolazepam (Telazol; Zoetis), atropine (Phoenix Pharmaceutical), and xylazine (AnaSed) and ventilated with inhaled isoflurane gas (Halocarbon Laboratories). No specific respiratory compensation strategy was used to account for breathing motion, but tidal volumes were reduced to 300–400 mL. Animals were positioned in the left lateral decubitus position, shaved, and a degassed water bath placed entirely over the ipsilateral ribcage (Fig. 1).

Histotripsy was performed using a 700 kHz preclinical research prototype system (HistoSonics, Inc.) as previously described [8, 10]. In each animal, a single 3 cm spherical hepatic ablation was prescribed. To initiate treatment, the acoustic driving voltage of the transducer was increased in step-wise fashion until a cavitation cloud was observed at the focal point. The automated robotic treatment parameters were adjusted to allow cooling pauses to minimize beam path heating in the ultrasound trajectory, resulting in a total treatment time of 75 min, longer than previously reported [7]. A comparison of histotripsy pulsing parameters to a previous subcostal liver study is shown in Table 1.

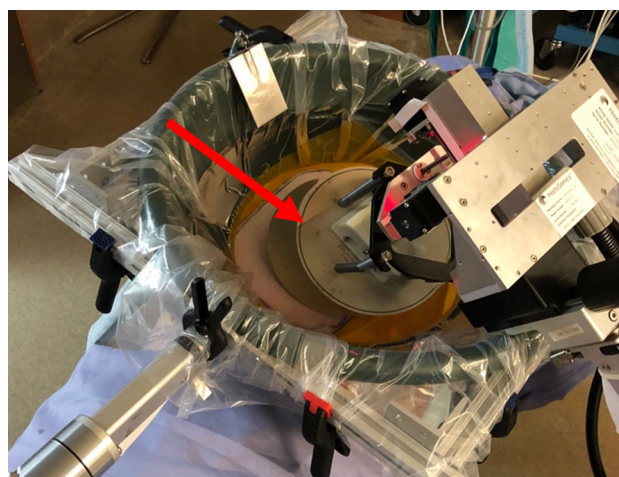


Fig. 1 Experimental setup. Therapy transducer (red arrow) is placed in coupling medium (degassed water bath) over the ipsilateral ribcage with the animal in the left lateral decubitus position

MR Imaging

Immediately following liver ablation, MR imaging of the abdomen was obtained in 5/6 cases with a single subject unable to be scanned due to unexpected human clinical use. Imaging was performed on a 3 T PET/MRI scanner (GE Signa PET/MR; GE Healthcare) using a dedicated body coil. A hepatocyte-specific gadolinium contrast agent (Eovist, Bayer Healthcare LLC) (0.05 mmol/kg at 2 mL/s) was used for dynamic contrast enhancement and hepatobiliary phase imaging. Imaging sequences included a localizing sequence, coronal SSFSE, axial T2-weighted fat-suppressed fast spin echo, diffusion weighted, and axial T1 weighted gradient recall echo. Axial T1 scans were performed pre-contrast and in the arterial, portal venous, and hepatobiliary phases.

Pathology

Following MRI, animals were euthanized with an intravenous injection of pentobarbital sodium and phenytoin sodium (Beuthanasia-D; Schering-Plough). The abdomen and thorax were inspected at necropsy by a certified veterinary technician and physician, and the liver, lower lobe of the right lung, and overlying body wall preserved in 10% buffered formalin for 8 weeks, sectioned and photographed. Representative samples from a cut through the mid ablation zone were placed in cassettes: two per ablation zone (superior and anterior ablation zone-boundary). One lung sample and one muscle sample from the overlying body wall were also taken for each animal. Tissue was processed in a Sakura Tissue-Tek VIP (Sakura Finetek), embedded with a Leica EG 1160 (Leica Biosystems), cut to 5 microns thick using a Leica RM2125RT (Leica

Table 1 Treatment parameters compared to a previous subcostal histotripsy study [7]

	Subcostal liver ablation (Smollock et al. [7])	Transcostal liver ablation
Prescribed ablation zone diameter	3.0 cm	3.0 cm
Treatment time	24 min 15 s	75 min
Duty cycle	< 1%	< 1%
Therapy “ON” time	50%	20%
Therapy transducer		
Diameter	20 cm	20 cm
Focal Length	14 cm	14 cm
Elements	18	18
Pulse sequence to generate cavitation	17–20 MPa	17–20 MPa
Pulse repetition frequency	600 Hz	600 Hz

Biosystems), and stained with hematoxylin and eosin. Slides were evaluated by a dedicated GI-hepatopathologist. The transition region between normal hepatic parenchyma and ablation zone was measured, qualitative descriptions provided, and digital microscopic photographs obtained of representative areas.

Data Analysis and Statistics

MRI findings were determined in consensus by two senior radiology residents with three and four years of experience in ablation research (PGY-4 and PGY-5) and a board-certified abdominal radiologist with 15-year experience. Technical success was determined by the creation of an ablation zone not significantly different from prescribed volume on MRI ($n = 5$) or pathology (in the single swine that did not undergo MRI). Three orthogonal measurements (craniocaudal (CC), anteroposterior (AP), and transverse (trans)) were taken of the ablation zone and volumes measured in 3D on portal venous phase imaging (Vitrea, Vital Images). Adjacent organs and structures were reviewed, with special attention to lung, body wall, ribs, and liver for any complications such as edema, thrombosis, and injury along the ultrasound beam path. Body wall edema and necrosis were classified as subcutaneous or muscular and then graded on a subjective severity scale (0 = none, 1 = trace, 2 = moderate, 3 = substantial). Lung edema/hemorrhage was graded similarly (0 = none, 1 = trace, 2 = moderate, and 3 = substantial). Portal and hepatic veins, bile ducts, and gallbladder were also inspected for injury.

Data analysis was performed using R version 3.4.4 (<http://www.r-project.org>). Given the small sample size, results would be underpowered with a t -test. Confidence intervals were therefore computed to estimate the true mean for ablation diameter and volume. Results outside of a 95% confidence interval were considered statistically

significant. Accelerated bootstrap confidence intervals with 5000 replicates are given for the mean diameter and volume.

Results

Histotripsy was technically successful in 6/6 animals with no deaths, complications, or signs of distress. Visualization of the echogenic bubble cloud throughout treatment was intermittent due to rib blockage of the diagnostic ultrasound (Fig. 2). When the bubble cloud was visible (i.e., the imaging probe was not blocked by ribs), it was observed at the expected focal location.

Ablation Zone (Fig. 3, Tables 2 and 3)

Ablation zones were within the confidence intervals of the prescribed volume ($13.8 \pm 1.8 \text{ cm}^3$ vs. 14.1 cm^3). The 95% confidence interval to estimate true volume was (12.41, 15.20, not different from prescribed). The ablation zone diameters were within the measurement error of the prescribed size (AP: $2.9 \pm 0.2 \text{ cm}$, CC: $3.1 \pm 0.3 \text{ cm}$, Trans: $3.0 \pm 0.1 \text{ cm}$ vs. prescribed 3.0 cm in all dimensions). The 95% CIs for mean diameter, AP (2.68, 3.20), CC (2.82, 3.29), and trans (2.94, 3.04), were not significantly different from the prescribed diameter. The average ablation zone depth was 5.8 cm, measured from the external abdominal wall to the center of the ablation zone. Ablation zones appeared similar to previous studies: hyperintense on T1 and T2WI with no internal enhancement, decreased peripheral perfusion, non-occlusive portal vein thrombus, and patent bile ducts within the ablation zone on delayed phase imaging [7, 8].

Histopathology was similar to previous studies as well with ablation zones near-completely necrotic and non-viable, narrow transition zones between central ablation and

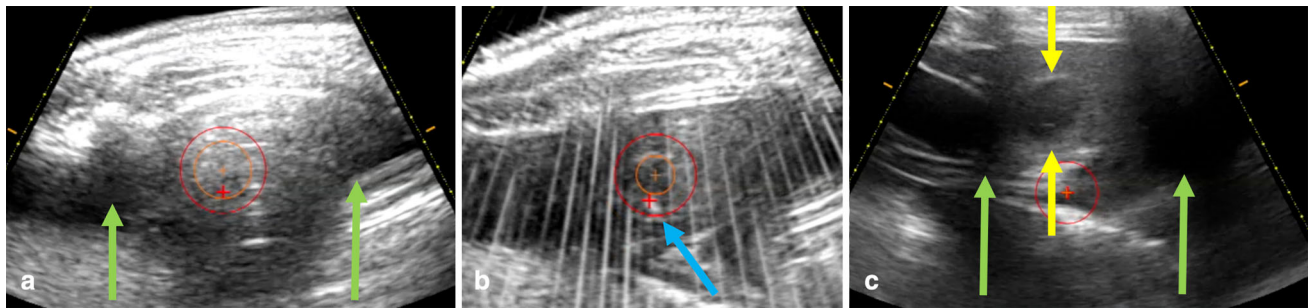


Fig. 2 Targeting and visualization of the echogenic bubble cloud. The red circle represents the target treatment volume. **a** Diagnostic US shows rib shadows (green arrows) during treatment planning. **b** Real-time tracking of the echogenic bubble cloud during transcostal ablation (blue arrow). At any point in time, the red “+” sign

indicated where the center of the bubble cloud is targeted. **c** Post-treatment ablation zone (yellow arrows) between rib shadows (green arrows; red circle is an artifact of image acquisition and does not represent treatment volume)

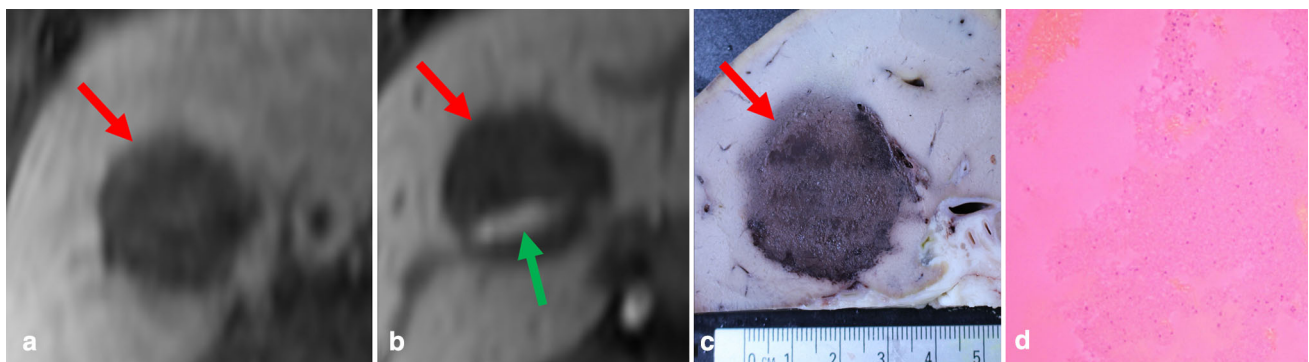


Fig. 3 Ablation zones. **a** Coronal post-contrast portal venous phase MRI image demonstrating a well demarcated ablation zone (red arrow). **b** Coronal post-contrast 20 min delayed image with Eovist demonstrating an intact bile duct (green arrow) traveling through the

ablation zone (red arrow). **c** Pathologic specimen demonstrating a sharp transition from the ablation zone (red arrow) to normal tissue. **d** Microscopic specimen (10x) of the center of the ablation zone demonstrates no residual viable tissue

Table 2 Mean ablation sizes

Diameter (prescribed = 3.0 cm)	<i>n</i> = 5
Anteroposterior (cm)	2.9 ± 0.2 cm
Craniocaudal (cm)	3.1 ± 0.3 cm
Transverse (cm)	3.0 ± 0.1 cm
Volume (cm ³ ; prescribed = 14.1 cm ³)	13.8 ± 1.8 cm ³
Transition zone	<i>n</i> = 6
Anterior (cm)	0.3 ± 0.1 cm
Superior (cm)	0.2 ± 0.2 cm

normal background liver (0.1–0.5 cm), and small arteries and bile ducts present within the ablation and transition zones (Fig. 4). The mean transition width on the anterior and superior aspects of the ablation was 0.3 ± 0.2 cm and 0.2 ± 0.2 cm, respectively.

Body Wall Edema (Fig. 5)

Intercostal muscle edema was seen in all 5 imaged subjects overlying the ablation zone (mean severity score = 1.6 ± 0.8). All 5 subjects displayed findings of T2 hyperintensity and enhancement consistent with muscle edema, but none of the subjects displayed additional edema within the subcutaneous soft tissues or skin. There was no evidence of body wall hemorrhage or necrosis. The ribs appeared normal.

At gross inspection, the edema/injury seen by MRI was not visible, and there was no histological evidence of injury.

Lung Injury (Fig. 6)

Four of the five subjects had imaging findings consistent with injury to the right lower lobe (mean of 1 × 2 × 4 cm) (mean severity score = 1.0 ± 0.7). The imaging appearance was similar to atelectatic enhancing lung along the path of the histotripsy beam. By imaging, one of the subjects had a moderate injury (severity

Table 3 Ablation imaging characteristics

	<i>n</i> = 5	Severity Score (0 = none, 1 = trace, 2 = moderate, and 3 = substantial)
Non-occlusive branch portal vein thrombus	4	n/a
Hepatic vein clot	0	n/a
Patent bile ducts in ablation zone	5	n/a
Body Wall Injury		
Subcutaneous edema	0	0.0
Muscle edema	5	1.6 ± 0.8
Muscle necrosis	0	0.0
Body wall hemorrhage	0	0.0
Lung Injury	4	1.0 ± 0.7

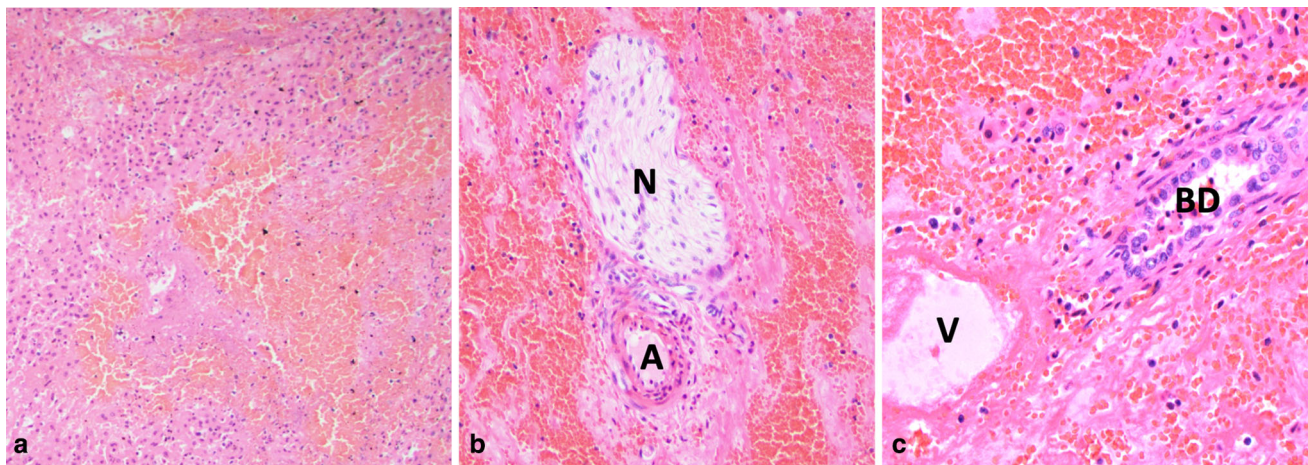


Fig. 4 Transition zone. **a** Microscopic image of transition zone (10×) demonstrates congestion, hemorrhage and some viable hepatocytes. **b** Transition zone (20×) with an intact artery (A) and nerve (N).

c Transition zone (40×) with an intact bile duct (BD) next to a necrotic vein (V)

score = 2), while the remaining three had mild areas of injury (severity score = 1). In the subject with moderate lung injury, there was sharp demarcation between injured and normal lung. There was no evidence of post-procedure pneumothorax, or hemothorax in any of the subjects.

At gross inspection, 5/6 subjects had a wedge-shaped visually red area of lung injury surrounded by normal appearing lung which corresponded to the MRI findings. Histopathology demonstrated hemorrhage in the alveolar space with bronchioles and blood vessels well-preserved. Pneumocytes lining alveoli within the areas of gross discoloration showed mild signs of injury. One animal did not have a lung lesion.

Discussion

Performing transcostal therapeutic ultrasound is challenging as the transducer and arrangement of piezoelectric elements is larger than a single interspace. Thus, some proportion of delivered ultrasound energy will inevitably be blocked by ribs, causing undesirable heating, reducing the energy that reaches the focus, and creating beam distortions and grating lobes. In previous studies, this has been avoided by using a subcostal approach [7, 8]. In this transcostal histotripsy study, we were able to use existing histotripsy parameters with minimal modification to achieve complete necrosis within the targeted tissue. Specific changes to previously described protocols included: (1) adjusting robotic treatment path algorithms to allow more cooling time, and (2) performing the treatment at a pressure level just above the cavitation threshold to ensure cavitation is only generated at the focus.

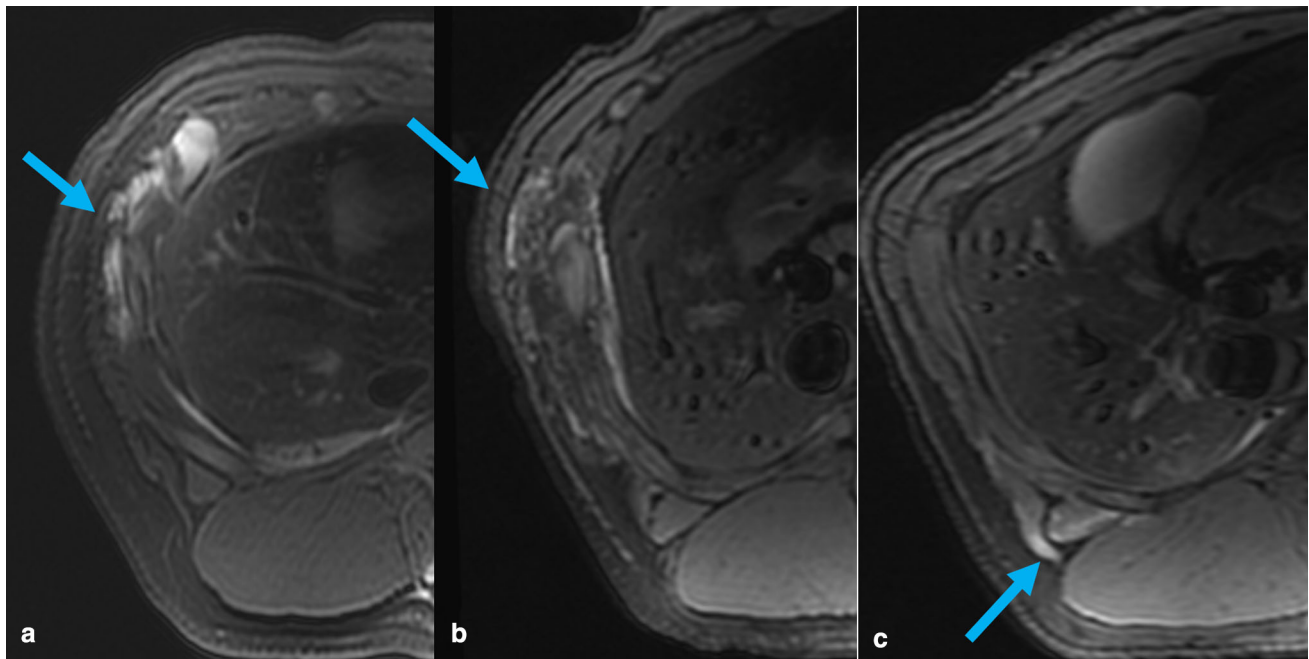


Fig. 5 Body wall edema post-histotripsy. Axial STIR images from three separate animals demonstrating body wall edema within the beam path (blue arrows). Body wall injury was not visible at necropsy and microscopic specimens demonstrated no histologic signs of damage

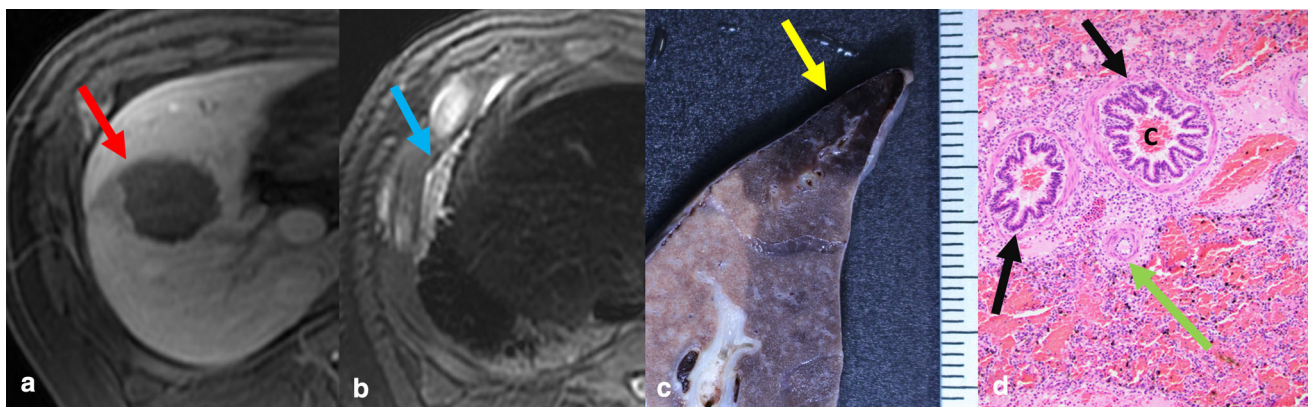


Fig. 6 Lung injury post-histotripsy. **a** Axial post-contrast portal venous phase MRI demonstrates an ablation zone within the right hepatic lobe (red arrow). **b** Axial T2 MRI superior to the ablation zone shows edema within the anterior aspect of the right lower lobe (blue arrow). **c** Gross pathology specimen of the right lower lobe

demonstrates discoloration of the lung corresponding to the MRI findings (yellow arrow). **d** Corresponding histopathologic specimen (20 \times) demonstrates an intact artery (green arrow) and intact bronchioles (black arrows) with alveolar congestion (C)

Using this approach, clinically relevant ($3 \times 3 \times 3$ cm prescription) transcostal ablation zones were created that had an equivalent size, precision, and imaging appearance when compared to subcostal ablations [7, 8]. Besides lengthening cooling intervals, the system was otherwise not specifically optimized for transcostal treatments, and therefore, minor body wall edema without pathologic correlate [7], and low-grade alveolar hemorrhage along the beam path were expected. The body wall edema was likely a reaction to sub-lethal elevations in temperature and only apparent on highly fluid-sensitive MRI pulse sequences.

The alveolar hemorrhage, similar to that encountered during lung biopsy [19], may be due more to the sensitivity of the lung to mechanical effects intrinsic to histotripsy than a thermal effect in which hemorrhage would not be expected to be a prominent feature [13].

Compared to thermal HIFU, histotripsy is less likely to cause body wall heating due to the extremely low duty cycle ($< 1\%$ for histotripsy compared to near continuous pulses for HIFU) and the threshold nature of tissue cavitation [20, 21]. However, body wall injury (thermal, not cavitation induced injury) can still occur with histotripsy

under certain conditions, such as in this study where large volume ablations were created through bone-containing acoustic windows [18, 22]. Unlike histotripsy, with thermal HIFU, there is no threshold effect, and tissue is heated along the entire beam path. However, any method that decreases HIFU thermal damage along the beam path will also result in reduction of focal temperatures. Due to this fundamental limitation, unintended injuries have been observed with thermal HIFU with reported cases of skin and muscle injuries, pain, rib necrosis and fractures [22–25]. More severe complications with HIFU include diaphragmatic rupture, biliary obstruction, pneumothorax, and pancreatico-duodenal fistulas, all suggesting that there is substantial pre-focal energy deposition [23, 25]. While these complications are likely to be less severe with histotripsy, this study was not a direct comparison of thermal HIFU and histotripsy.

Improved device features and strategies currently in development are expected to substantially shorten treatment duration. For instance, aberration correction to minimize beam distortion is being actively investigated [26, 27], as is the development of array transducers in which elements that are obstructed by ribs or air could be turned off, thus reducing delivery of thermal energy that is not contributing to cavitation at the focus [28]. By way of comparison, thermal HIFU is associated with prolonged treatment times depending on ablation zone size, patient factors, ultrasound window, etc., with times as long as 5 h (range 8–685 min) reported in the literature [23, 24, 29].

A limitation of transcostal histotripsy procedures is the limited visualization of the bubble cloud throughout the ablation, due to the ultrasound window for the diagnostic transducer being intermittently blocked by ribs [7, 15]. Importantly, even without direct visualization of the bubble cloud for the entirety of the treatment, the ablation zones maintained fidelity to prescribed size and shape, likely due to the robotic control of the treatment path. Additional future developments including CT or MR fusion to the diagnostic US and cavitation mapping using passive cavitation detection may be helpful to aid in targeting and real-time treatment feedback [30, 31].

This study had additional limitations, including the use of a non-tumor bearing animal model. Large animal tumor models are scarce and difficult to obtain, thus, to date, domestic pigs have served successfully as a preclinical model in multiple prior ablation studies [32, 33]. Other limitations include the lack of any type of respiratory compensation which could result in elongated ablation zones in the craniocaudal dimension, and the limited intercostal spaces using the transcostal ultrasound window in pigs as compared to humans. This study was also an acute non-survival study but appears appropriate to determine the safety and efficacy of transcostal histotripsy

ablation, similar to prior studies [7, 8, 10]. Lastly, only one modified treatment protocol was studied without temperature data. Optimizing the method used in this study and comparing to other treatment protocols using thermal data may be warranted.

Conclusion

Transcostal hepatic histotripsy appears feasible, effective, and no severe injuries were identified in this acute pre-clinical study performed with a non-optimized, prototype system. In the future, aberration correction and multi-element arrays are expected to reduce treatment time and, along with optimization of treatment protocols, are expected to further decrease the minor tissue injuries along the beam path found in this study.

Acknowledgements The authors of this study would like to acknowledge the HistoSonics R&D team (Josh Stopek PhD, Jon Cannata PhD, Ryan Miller PhD, and Alex Duryea PhD) and the animal anesthesia and care team.

Declarations

Conflict of interest This study has received funding from HistoSonics, Inc. (Ann Arbor, MI). Author EV is a consultant, stockholder, and receives research support from HistoSonics, Inc. Author ZX is a stockholder and receives research support from HistoSonics, Inc. Author PL is a consultant and stockholder with HistoSonics, Inc., a consultant with NeuWave/Ethicon, Inc., and receives research support from Siemens Healthineers. Author TH is a consultant, stockholder, and receives research support from HistoSonics, Inc. Author FL is a consultant, stockholder, receives research support, and is on the board of directors at HistoSonics, Inc., is a consultant with Ethicon, Inc., and has patents and royalties with Medtronic, Inc. Author TZ is a consultant, stockholder, receives research support from HistoSonics, Inc. and is a consultant with Ethicon, Inc.)

Informed consent All applicable international, national, and/or institutional guidelines for the care and use of animals were followed. All procedures performed in studies involving animals were in accordance with the ethical standards of the institution or practice at which the studies were conducted. For this type of study, informed consent is not required. For this type of study, consent for publication is not required.

References

1. Knavel EM, Brace CL. Tumor ablation: common modalities and general practices. *Tech Vasc Interv Radiol*. 2013;16:192–200. <https://doi.org/10.1053/j.tvir.2013.08.002>.
2. Poon RT, Ng KK, Lam CM, et al. Learning curve for radiofrequency ablation of liver tumors: prospective analysis of initial 100 patients in a tertiary institution. *Ann Surg*. 2004;239:441–9.
3. Livraghi T, Solbiati L, Meloni MF, et al. Treatment of focal liver tumors with percutaneous radio-frequency ablation: complications encountered in a multicenter study. *Radiology*. 2003;226:441–51. <https://doi.org/10.1148/radiol.2262012198>.

4. Parsons JE, Cain CA, Abrams GD, Fowlkes JB. Pulsed cavitation ultrasound therapy for controlled tissue homogenization. *Ultrasound Med Biol.* 2006;32:115–29. <https://doi.org/10.1016/j.ultrasmedbio.2005.09.005>.
5. Xu Z, Ludomirsky A, Eun LY, et al. Controlled ultrasound tissue erosion. *IEEE Trans Ultrason Ferroelectr Freq Control.* 2004;51:726–36.
6. Vlasisavljevich E, Lin K-W, Maxwell A, et al. Effects of Ultrasound Frequency and Tissue Stiffness on the Histotripsy Intrinsic Threshold for Cavitation. *Ultrasound Med Biol.* 2015;41:1651–67. <https://doi.org/10.1016/j.ultrasmedbio.2015.01.028>.
7. Smolock AR, Cristescu MM, Vlasisavljevich E, et al. Robotically Assisted Sonic Therapy as a Noninvasive Nonthermal Ablation Modality: Proof of Concept in a Porcine Liver Model. *Radiology.* 2018;287:485–93. <https://doi.org/10.1148/radiol.2018171544>.
8. Longo KC, Knott EA, Watson RF, et al. Robotically Assisted Sonic Therapy (RAST) for Noninvasive Hepatic Ablation in a Porcine Model: Mitigation of Body Wall Damage with a Modified Pulse Sequence. *Cardiovasc Intervent Radiol.* 2019;42:1016–23. <https://doi.org/10.1007/s00270-019-02215-8>.
9. Lundt JE, Allen SP, Shi J, et al. Non-invasive, Rapid Ablation of Tissue Volume Using Histotripsy. *Ultrasound Med Biol.* 2017;43:2834–47. <https://doi.org/10.1016/j.ultrasmedbio.2017.08.006>.
10. Knott EAEA, Swietlik JFJF, Longo KCKC, et al. Robotically-Assisted Sonic Therapy for Renal Ablation in a Live Porcine Model: Initial Preclinical Results. *J Vasc Interv Radiol.* 2019;30:1293–302. <https://doi.org/10.1016/j.jvir.2019.01.023>.
11. Vlasisavljevich E, Kim Y, Allen S, et al. Image-guided non-invasive ultrasound liver ablation using histotripsy: feasibility study in an in vivo porcine model. *Ultrasound Med Biol.* 2013;39:1398–409. <https://doi.org/10.1016/j.ultrasmedbio.2013.02.005>.
12. Roberts WW, Hall TL, Ives K, et al. Pulsed Cavitation Ultrasound: A Noninvasive Technology for Controlled Tissue Ablation (Histotripsy) in the Rabbit Kidney. *J Urol.* 2006;175:734–8. [https://doi.org/10.1016/S0022-5347\(05\)00141-2](https://doi.org/10.1016/S0022-5347(05)00141-2).
13. Vlasisavljevich E, Kim Y, Owens G, et al. Effects of tissue mechanical properties on susceptibility to histotripsy-induced tissue damage. *Phys Med Biol.* 2013;59:253–70. <https://doi.org/10.1088/0031-9155/59/2/253PMID-24351722>.
14. Hall TL, Kieran K, Ives K, et al. Histotripsy of rabbit renal tissue in vivo: temporal histologic trends. *J Endourol.* 2007;21:1159–66. <https://doi.org/10.1089/end.2007.9915>.
15. Vlasisavljevich E, Maxwell A, Mancia L, et al. Visualizing the Histotripsy Process: Bubble Cloud-Cancer Cell Interactions in a Tissue-Mimicking Environment. *Ultrasound Med Biol.* 2016;42:2466–77. <https://doi.org/10.1016/j.ultrasmedbio.2016.05.018>.
16. Lake AM, Xu Z, Wilkinson JE, et al. Renal Ablation by Histotripsy—Does it Spare the Collecting System? *J Urol.* 2008;179:1150–4. <https://doi.org/10.1016/j.juro.2007.10.033>.
17. Roberts WW. Development and translation of histotripsy: current status and future directions. *Curr Opin Urol.* 2014;24:104–10. <https://doi.org/10.1097/MOU.0000000000000001>.
18. Kim Y, Vlasisavljevich E, Owens GE, et al. *In vivo* transcostal histotripsy therapy without aberration correction. *Phys Med Biol.* 2014;59:2553–68. <https://doi.org/10.1088/0031-9155/59/11/2553>.
19. Heerink WJ, de Bock GH, de Jonge GJ, et al. Complication rates of CT-guided transthoracic lung biopsy: meta-analysis. *Eur Radiol.* 2017;27:138–48. <https://doi.org/10.1007/s00330-016-4357-8>.
20. ter Haar G. Acoustic Surgery. *Phys Today.* 2001;54:29–34. <https://doi.org/10.1063/1.1445545>.
21. Yu H, Burke CT. Comparison of Percutaneous Ablation Technologies in the Treatment of Malignant Liver Tumors. *Semin Interv Radiol.* 2014;31:129–37. <https://doi.org/10.1055/s-0034-1373788>.
22. Quesson B, Merle M, Köhler MO, et al. A method for MRI guidance of intercostal high intensity focused ultrasound ablation in the liver. *Med Phys.* 2010;37:2533–40. <https://doi.org/10.1118/1.3413996>.
23. Jung SE, Cho SH, Jang JH, Han J-Y. High-intensity focused ultrasound ablation in hepatic and pancreatic cancer: complications. *Abdom Imaging.* 2011;36:185–95. <https://doi.org/10.1007/s00261-010-9628-2>.
24. Fischer K, Gedroyc W, Jolesz FA. Focused Ultrasound as a Local Therapy for Liver Cancer. *Cancer J.* 2010;16:118–24. <https://doi.org/10.1097/PPO.0b013e3181db7c32>.
25. Wu F, Wang Z-B, Chen W-Z, et al. Extracorporeal high intensity focused ultrasound ablation in the treatment of 1038 patients with solid carcinomas in China: an overview. *Ultrason Sonochem.* 2004;11:149–54. <https://doi.org/10.1016/j.ultsonch.2004.01.011>.
26. Macoskey JJ, Hall TL, Sukovich JR, et al. Soft-Tissue Aberration Correction for Histotripsy. *IEEE Trans Ultrason Ferroelectr Freq Control.* 2018;65:2073–85. <https://doi.org/10.1109/TUFFC.2018.2872727>.
27. Gerhardson T, Sukovich JR, Pandey AS, et al. Catheter Hydrophone Aberration Correction for Transcranial Histotripsy Treatment of Intracerebral Hemorrhage: Proof-of-Concept. *IEEE Trans Ultrason Ferroelectr Freq Control.* 2017;64:1684–97. <https://doi.org/10.1109/TUFFC.2017.2748050>.
28. Wang TY, Xu Z, Hall TL, et al. Active focal zone sharpening for high-precision treatment using histotripsy. *IEEE Trans Ultrason Ferroelectr Freq Control.* 2011;58:305–15. <https://doi.org/10.1109/TUFFC.2011.1808>.
29. Li J-J, Xu G-L, Gu M-F, et al. Complications of high intensity focused ultrasound in patients with recurrent and metastatic abdominal tumors. *World J Gastroenterol.* 2007;13:2747–51. <https://doi.org/10.3748/WJG.V13.I19.2747>.
30. Bader KB, Haworth KJ, Maxwell AD, Holland CK. Post Hoc Analysis of Passive Cavitation Imaging for Classification of Histotripsy-Induced Liquefaction in Vitro. *IEEE Trans Med Imaging.* 2018;37:106–15. <https://doi.org/10.1109/TMI.2017.2735238>.
31. Anthony GJ, Bollen V, Hendley S, et al. Assessment of histotripsy-induced liquefaction with diagnostic ultrasound and magnetic resonance imaging in vitro and ex vivo. *Phys Med Biol.* 2019;64. <https://doi.org/10.1088/1361-6560/ab143f>.
32. Hansen PD, Rogers S, Corless CL, et al. Radiofrequency ablation lesions in a pig liver model. *J Surg Res.* 1999. <https://doi.org/10.1006/jsre.1999.5709>.
33. Brace CL, Laeseke PF, Sampson LA, et al. Microwave ablation with a single small-gauge triaxial antenna: In vivo porcine liver model. *Radiology.* 2007;242:435–40. <https://doi.org/10.1148/radiol.2422051411>.

Publisher's Note Springer Nature remains neutral with regard to jurisdictional claims in published maps and institutional affiliations.